# Parity-time-symmetry breaking in double-slab surface-plasmon-polariton waveguides

**Youngsun Choi,[1] Jong-Kyun Hong,[2] Jin-Ho Cho,[1] Kwang-Geol Lee,[1] Jae Woong Yoon,[1] and Seok Ho Song[1,*]**

*[1]Department of Physics, Hanyang University, Seoul 133-791, South Korea*
*[2]Department of Electrical Eng., Hanyang University, Seoul 133-791, South Korea*
*[*]shsong@hanyang.ac.kr*

**Abstract:** We theoretically demonstrate spontaneous PT-symmetry breaking behavior of surface-plasmon polaritons (SPP) in coupled double-slab (DS) waveguides. By virtue of a flat-top field at critical wavelength, the imaginary index of a DS-SPP mode can be controlled via changing the core thickness, while the real index is kept constant. Therefore, a waveguide coupler that consists of a pair of DS-SPP waveguides with different core thicknesses can represent a passive PT-symmetric system, which always maintains symmetry under a real potential. This set-up also represents a good opportunity to investigate the underlying physics of PT-symmetry breaking in non-Hermitian Hamiltonian systems.

**OCIS codes:** (240.6680) Surface plasmons; (230.7400) Waveguides, slab; (080.6755) Systems with special symmetry.

## References and links

1.  C. M. Bender and S. Boettcher, "Real Spectra in Non-Hermitian Hamiltonians Having PT Symmetry," Phys. Rev. Lett. **80**(24), 5243–5246 (1998).
2.  S. Klaiman, U. Günther, and N. Moiseyev, "Visualization of Branch Points in PT-Symmetric Waveguides," Phys. Rev. Lett. **101**(8), 080402 (2008).
3.  A. Guo, G. J. Salamo, D. Duchesne, R. Morandotti, M. Volatier-Ravat, V. Aimez, G. A. Siviloglou, and D. N. Christodoulides, "Observation of PT-Symmetry Breaking in Complex Optical Potentials," Phys. Rev. Lett. **103**(9), 093902 (2009).
4.  C. E. Rüter, K. G. Makris, R. El-Ganainy, D. N. Christodoulides, M. Segev, and D. Kip, "Observation of parity–time symmetry in optics," Nat. Phys. **6**(3), 192–195 (2010).
5.  B. Peng, Ş. K. Özdemir, F. Lei, F. Monifi, M. Gianfreda, G. L. Long, S. Fan, F. Nori, C. M. Bender, and L. Yang, "Parity–time-symmetric whispering-gallery microcavities," Nat. Phys. **10**(5), 394–398 (2014).
6.  B. Peng, K. Ozdemir, S. Rotter, H. Yilmaz, M. Liertzer, F. Monifi, C. M. Bender, F. Nori, and L. Yang, "Loss-induced suppression and revival of lasing," Science **346**(6207), 328–332 (2014).
7.  H. Jing, S. K. Özdemir, X. Y. Lü, J. Zhang, L. Yang, and F. Nori, "PT-symmetric phonon laser," Phys. Rev. Lett. **113**(5), 053604 (2014).
8.  L. Feng, Y. L. Xu, W. S. Fegadolli, M. H. Lu, J. E. B. Oliveira, V. R. Almeida, Y. F. Chen, and A. Scherer, "Experimental demonstration of a unidirectional reflectionless parity-time metamaterial at optical frequencies," Nat. Mater. **12**(2), 108–113 (2012).
9.  A. Regensburger, C. Bersch, M. A. Miri, G. Onishchukov, D. N. Christodoulides, and U. Peschel, "Parity-time synthetic photonic lattices," Nature **488**(7410), 167–171 (2012).
10. Z. H. Musslimani, K. G. Makris, R. El-Ganainy, and D. N. Christodoulides, "Optical Solitons in PT Periodic Potentials," Phys. Rev. Lett. **100**(3), 030402 (2008).
11. Y. D. Chong, L. Ge, and A. D. Stone, "PT-Symmetry Breaking and Laser-Absorber Modes in Optical Scattering Systems," Phys. Rev. Lett. **106**(9), 093902 (2011).
12. L. Feng, Z. J. Wong, R.-M. Ma, Y. Wang, and X. Zhang, "Single-mode laser by parity-time symmetry breaking," Science **346**(6212), 972–975 (2014).
13. C. M. Bender, D. C. Brody, and H. F. Jones, "Complex Extension of Quantum Mechanics," Phys. Rev. Lett. **89**(27), 270401 (2002).
14. C. M. Bender, "Making sense of non-Hermitian Hamiltonians," Rep. Prog. Phys. **70**(6), 947–1018 (2007).
15. W. D. Heiss, "The physics of exceptional points," J. Phys. A **45**, 444016 (2012).
16. R. El-Ganainy, K. G. Makris, D. N. Christodoulides, and Z. H. Musslimani, "Theory of coupled optical PT-symmetric structures," Opt. Lett. **32**(17), 2632–2634 (2007).
17. A. Lupu, H. Benisty, and A. Degiron, "Switching using PT symmetry in plasmonic systems: positive role of the losses," Opt. Express **21**(18), 21651–21668 (2013).

18. J. Yoon, S. H. Song, and S. Park, "Flat-top surface plasmon-polariton modes guided by double-electrode structures," Opt. Express **15**(25), 17151–17162 (2007).
19. H. Benisty and M. Besbes, "Confinement and optical properties of the plasmonic inverse-rib waveguide," J. Opt. Soc. Am. B **29**(4), 818 (2012).
20. H. Benisty, C. Yan, A. Degiron, and A. Lupu, "Healing Near-PT-Symmetric Structures to Restore Their Characteristic Singularities: Analysis and Examples," J. Lightwave Technol. **30**(16), 2675–2683 (2012).
21. Y. Li, X. Guo, L. Chen, C. Xu, J. Yang, X. Jiang, and M. Wang, "Coupled Mode Theory Under The Parity-Time Symmetry Frame," J. Lightwave Technol. **31**(15), 2477–2481 (2013).
22. M. G. Blaber, M. D. Arnold, and M. J. Ford, "Search for the Ideal Plasmonic Nanoshell: The Effects of Surface Scattering and Alternatives to Gold and Silver," J. Phys. Chem. C **113**(8), 3041–3045 (2009).
23. C. M. Bender, M. Gianfreda, Ş. K. Özdemir, B. Peng, and L. Yang, "Twofold transition in PT -symmetric coupled oscillators," Phys. Rev. A. **88**, 1–8 (2013).
24. H. Ramezani, J. Schindler, F. M. Ellis, U. Günther, and T. Kottos, "Bypassing the bandwidth theorem with PT symmetry," Phys. Rev. A **85**(6), 062122 (2012).

## 1. Introduction

Hermitian Hamiltonians are known to have real eigenvalues. The inverse, however, is not necessarily true. In a seminal work by Bender and Boettcher [1], it was shown that non-Hermitian Hamiltonians can potentially have real eigenvalues if they have parity-time (PT) symmetry. Interestingly, it is possible to mimic PT-symmetry in optics. So far, many different optical systems, including waveguide couplers [2–4], microcavities [5–7], Bragg gratings [8], optical lattices [9,10], and lasers [11,12], have been demonstrated to mimic PT-symmetry. Many of these studies have focused on the spontaneous PT-symmetry breaking and concomitant phenomena [2,13–15]. Formal equivalence of Schrödinger equation with electromagnetic wave equation under paraxial approximation dictates that the refractive index $n$ corresponds to the potential energy $V$ in the Hamiltonian [16]. Therefore, the condition $V(x) = V^*(-x)$ for PT-symmetric Hamiltonians implies $n(x) = n^*(-x)$ for PT-symmetric optical systems. In a coupled-waveguide system, for example, the real values of the refractive index should be the same in both channels. Conversely, the imaginary values have opposite signs, implying balanced gain (channel 1) and loss (channel 2) conditions. Designing such a system in experiments is not straightforward because of practical difficulty in systematical control of the gain and loss in both channels.

The gauge transformation can alleviate the strictness of the balanced gain/loss conditions. Even when two channels have different losses, but no gain, the virtual-zero level can be shifted to the average value of the loss to satisfy the PT-symmetric condition [3,17]. A system satisfying this modified condition is so-called a passive PT-symmetric system. However, the passive PT-symmetry still requires the ability to separately control the imaginary indices (amount of loss) of two channels while keeping the real indices constant in both channels. Unfortunately, in most cases, the real index simultaneously changes when the waveguide structure is tuned to control the losses (imaginary index). Therefore, in optical PT-symmetry studies, it is crucial to independently control the real and imaginary indices.

To this end, we suggest double-slab (DS) surface-plasmon-polariton (SPP) waveguides as a test-bench of PT-symmetry. The proposed DS-SPP waveguide system consists of stacked multi-layers of metals (M) and insulators (I) in the sequence of IMIMI. In this particular waveguide geometry, there exists a critical wavelength where the effective imaginary index ($Im\{n_{eff}\}$) of the mode is inversely proportional to core dielectric thickness while the effective real index ($Re\{n_{eff}\}$) remains constant [18]. This condition is obtained for a *flat-top long-range SPP mode* at a critical wavelength $\lambda_c$. Therefore, coupled DS-SPP waveguides with two different core thicknesses act as a passive PT-symmetric system. In this study, we utilize this unique property to theoretically study the spontaneous PT-symmetry breaking in coupled DS-SPP waveguides.

## 2. System design

Figure 1(a) shows the schematic of a single DS-SPP waveguide (inset) and the effective propagation index of the SPP mode as a function of the core diameter $D$ for system

parameters $n_c = 1.47$, $n_d = 1.45$, and metal (Au) thickness $t = 20$ nm. A DS-SPP waveguide is characterized by the dispersion relation

$$\frac{\alpha_m \alpha_d}{\varepsilon_m \varepsilon_d} + \frac{\alpha_c \alpha_m}{\varepsilon_c \varepsilon_m} \tan h(\alpha_c D / 2) + \left(\frac{\alpha_m}{\varepsilon_m}\right)^2 \tan h(\alpha_m t) + \frac{\alpha_d \alpha_c}{\varepsilon_d \varepsilon_c} \tan h(\alpha_c D / 2) \tan h(\alpha_m t) = 0, \quad (1)$$

where $\alpha_i = (\beta^2 - \varepsilon_i k_0^2)^{1/2}$ ($i = m, d \ or \ c$) [18]. Here, subscripts $m$, $d$ and $c$ denote the metal, cladding, and core, respectively. This dispersion relation implies the critical wavelength $\lambda_c$ determined by

$$\frac{1}{\lambda_c} = \frac{1}{2\pi t} \frac{1}{\left[\varepsilon_c - \varepsilon_m(\lambda_c)\right]^{1/2}} \tan h^{-1}\left(-\frac{\varepsilon_m(\lambda_c)}{\varepsilon_d}\left[\frac{\varepsilon_c - \varepsilon_d}{\varepsilon_c - \varepsilon_m(\lambda_c)}\right]^{1/2}\right), \quad (2)$$

for the flat-top mode [18]. In our case shown in Fig. 1(a), the critical wavelength $\lambda_c$ is 925.7 nm. As expected, the calculated real effective index $Re\{n_{eff}\}$ remains constant while the imaginary effective index $Im\{n_{eff}\}$ monotonically decreases with increasing $D$. We note that this unique property is absent in other coupled-waveguide systems which were considered by Benisty *et al.* [19,20]. In general, adding additional materials to introduce unbalanced losses inevitably cause changes in the boundary conditions and finally affect change in both real and imaginary effective indices.
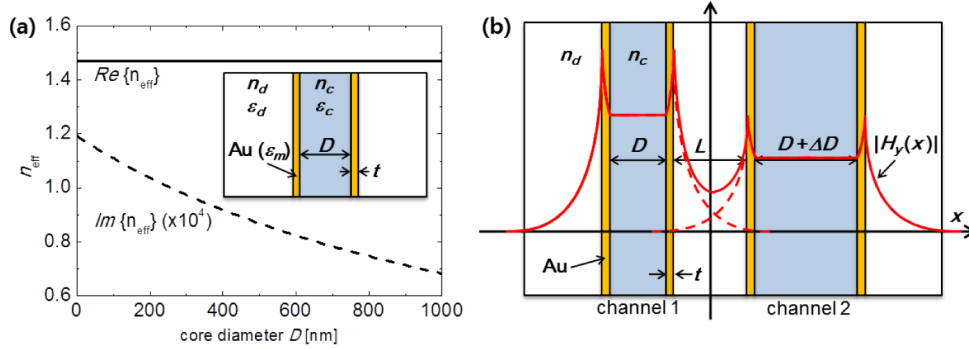


Fig. 1. (a) Real and imaginary effective indices of the SPP mode guided in a DS-SPP waveguide (inset) as a function of the core diameter $D$. System parameters are $n_c = 1.47$, $n_d = 1.45$, and metal(Au) thickness $t = 20$ nm. (b) Coupled DS-SPP waveguide structure having a separation distance of $L$. The core diameter of channel 2 is larger than that of channel 1 by $\Delta D$. The cross-sectional field profiles are indicated by red curves (solid for the coupled mode and dashed for uncoupled modes). For these profiles, we use $D = 100$ nm and $L = 5.5$ μm.

We further consider coupled double DS-SPP waveguide systems for a passive PT-symmetric system as shown in Fig. 1(b). The two DS-SPP waveguides have the same system parameters, with the exception of the core diameter $D$. In this configuration, $Re\{n_{eff}\}$ is identical in both channels while $Im\{n_{eff}\}$ is different. The core diameter of channel 2 is larger than that of channel 1 by $\Delta D$. With increasing $\Delta D$, the difference in $Im\{n_{eff}\}$ between the two channels gradually increases (Fig. 1(a)). This property provides an effective PT parameter tuning method that corresponds to the gain and loss control in the active PT-symmetric systems. In the following sections, we provide a detailed theory of this passive PT-symmetric system and show how the passive PT-symmetry breaking occurs in our proposed systems.

## 3. Coupled mode theory and passive PT-symmetry breaking

We apply the standard coupled-mode formalism [21] for studying passive PT-symmetry breaking in coupled DP-SPP waveguides. The total field of the system can be described with

wave function $\Psi(x,z) = \Sigma_{n\,=\,1,2}\,A_n(z)\phi_n(x)$, where $\phi_n(x)$ is the mode field in channel $n$ for the uncoupled case. Coupling between the waveguide channels follows the equation [3]

$$i\frac{d}{dz}\begin{bmatrix} A_1 \\ A_2 \end{bmatrix} = \begin{bmatrix} (\beta+i\alpha_1)+\delta_1 & \kappa_{12} \\ \kappa_{21} & (\beta+i\alpha_2)+\delta_2 \end{bmatrix}\begin{bmatrix} A_1 \\ A_2 \end{bmatrix} \qquad (3)$$

Here, $\beta$ and $\alpha$ are the uncoupled real and imaginary propagation constants, respectively. Modifications due to the inter-channel coupling are described by parameters: $\kappa_{nm}$ (coupling constant) and $\delta_n$ (correction to the propagation constant). Eigenvalues of Eq. (3) are

$$\lambda_\pm = \beta + i\alpha_M + \delta_M \pm \sqrt{(i\alpha_D + \delta_D)^2 + \kappa_{12}\kappa_{21}} \qquad (4)$$

Here, $\lambda_+$ is the propagation constant of the symmetric mode ($\Psi_+$) and $\lambda_-$ is that of the anti-symmetric mode ($\Psi_-$), where $\delta_M = (\delta_1 + \delta_2)/2$, $\delta_D = (\delta_1 - \delta_2)/2$, $\alpha_M = (\alpha_1 + \alpha_2)/2$, and $\alpha_D = (\alpha_1 - \alpha_2)/2$. Note that $\beta$ and $\alpha$ are real valued, while $\delta$ and $\kappa$ are complex valued. For an exact PT-symmetric case, where the gain and loss are matched to compensate for one another, there is no net propagation loss. This indicates that $\lambda_+$ and $\lambda_-$ are both real. Additionally, at the PT-symmetry-breaking threshold, the propagation constants of eigen modes converge to each other. From Eq. (4), this condition is satisfied when $\alpha_M = \delta_D = 0$ and $-\alpha_D^2 + \kappa_{12}\kappa_{21} = 0$.. Beyond the threshold, the two eigen modes have different decay constants (imaginary propagation constants) but the same real propagation constants.
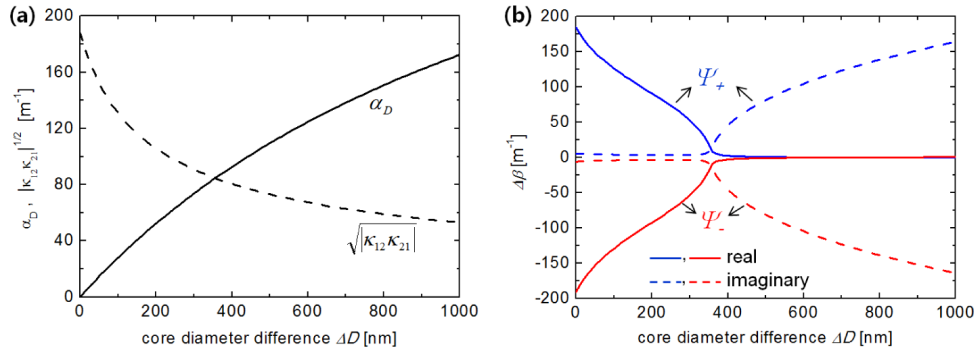


Fig. 2. (a) $\alpha_D$ (solid) and $|\kappa_{12}\kappa_{21}|^{1/2}$ (dashed) as a function of $\Delta D$. (b) Real (solid) and imaginary (dashed) values of $\Delta\beta$. Symmetric and anti-symmetric modes are indicated by blue and red curves, respectively.

To estimate the threshold in our system, we calculate $|\kappa_{12}\kappa_{21}|^{1/2}$ and $\alpha_D$ as a function of the difference in the core diameters $\Delta D$. The result is shown in Fig. 2(a). We use fixed system parameters $n_c = 1.47$, $n_d = 1.45$, $t = 20$ nm, $D = 100$ nm, and $L = 5.5$ μm while $\Delta D$ varies from 0 to 1000 nm. The critical wavelength for the flat-top mode is 925.7 nm and the permittivity of Au at that wavelength is $\varepsilon_m(\lambda_c = 925.7\ \text{nm}) = 39.8 + 0.56i$ [22]. The spontaneous PT-symmetry breaking occurs around $\Delta D = 350$ nm where the magnitudes of $\alpha_D$ and $|\kappa_{12}\kappa_{21}|^{1/2}$ become identical. In contrast to exact PT-symmetric systems, the threshold in our case respecting a gauge-transformed, passive PT-symmetry is not clearly defined. This smoothening effect of the phase transition point is caused by the following two reasons. First, as a dominant cause, $\kappa_{12}$ and $\kappa_{21}$ cannot have exactly opposite phases and consequently $\text{Im}\{\kappa_{12}\kappa_{21}\} \neq 0$. This is because both channels in coupled DS-SPP waveguides only experience losses. The resultant smoothening of the transition point revealed in Fig. 2(b) agrees well with the general properties previously explained by Bender *et al.* [23] and Benisty *et al.* [19]. Second, as found in the field profile (Fig. 1(b)), different modal field amplitudes invade into the other channel, causing the channels to react differently to one another such that $(\delta_1 - \delta_2)/2 = \delta_D \neq 0$.

Figure 2(b) shows propagation constants of the symmetric ($\Psi_+$) and anti-symmetric ($\Psi_-$). To clarify the PT-symmetry breaking behavior, we show the difference between the propagation constant and the mean value, i.e., $\Delta\beta_\pm = \lambda_\pm - \beta - i\alpha_M - \delta_M$. The blue-colored symmetric and red-colored anti-symmetric modes are shown in their real (solid) and imaginary (dashed) values. For small $\Delta D$ ($< 350$ nm), the two modes have large discrepancies in their real propagation constants and small differences in their imaginary propagation constants. Additionally, around the threshold value ($\Delta D \approx 350$ nm), the real propagation constants become closer to each other while the imaginary propagation constants start to become separated. This demonstrates the evolution of the system from the unbroken PT-symmetry phase into the broken PT-symmetry phase. As shown in Fig. 2(b), the converging point of the real propagation constants and the diverging point of the imaginary constants do not coincide with each other. This is dissimilar from an ideal PT-symmetric system. This is because $\delta_D$ and Im$\{\kappa_{12}\kappa_{21}\}$ in Eq. (4) are non-zero in our system as discussed earlier. The non-zero values of $\delta_D$ and Im$\{\kappa_{12}\kappa_{21}\}$ that appear in most passive PT-symmetric systems cause deviations in the symmetry breaking behaviors from those occurring in ideal PT-symmetric systems. This deviation can be alleviated by appropriately adjusting $\delta_M$ as discussed by Benisty *et al.* [20]. Nonetheless, the features of PT-symmetry breaking are clearly found in our case.

## 4. State evolution and inter-channel power transfer
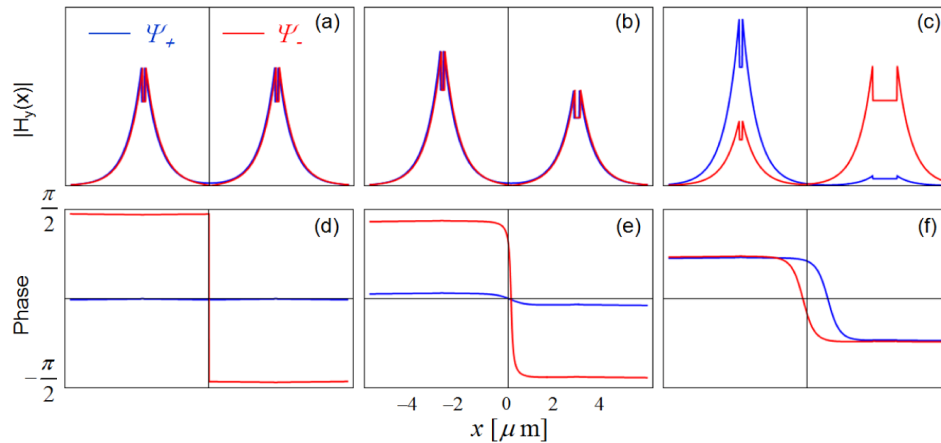


Fig. 3. Cross-sectional field magnitude $|H_y|$ profiles of eigen modes for (a) $\Delta D = 0$, (b) 100 nm, and (c) 900 nm. Phase arg($H_y$) profiles of eigen modes for (d) $\Delta D = 0$, (e) 100 nm, and (f) 900 nm. Symmetric (symmetric-like) and anti-symmetric (anti-symmetric-like) modes are in blue and red, respectively.

Cross-sectional field profiles and the phases of eigen modes for three representative $\Delta D$ values are shown in Fig. 3. For $\Delta D = 0$, the field profiles of the two modes are identical and the associated phase profile shows exact symmetry (blue) and anti-symmetry (red) as shown in Figs. 3(a) and 3(d). At $\Delta D = 100$ nm, the field profiles of the two eigen modes are still almost identical (b); however, as can be seen from the phase in (e), they are no longer perfectly symmetric nor anti-symmetric. Far beyond the threshold ($\Delta D = 900$ nm), the two modes show remarkable difference in the magnitude while the phase values become similar between the two modes. These are typical properties of PT-symmetric systems.

Figure 4 shows the evolution of the mode. The oscillatory behavior is caused by the interference between the two eigen modes. The field amplitudes are normalized by the instantaneous total power to clearly visualize the evolution. As $\Delta D$ increases, the difference in the real propagation constants of the two modes gets smaller and forms a longer beating period in the power oscillation. This effect is consistent with diverging beat length with the

merging real eigen values beyond symmetry-breaking threshold as shown in Fig. 2(b). In the region of $\Delta D$ < 350 nm, the two modes have similar decay constants (imaginary); therefore, power oscillations are clearly observed during propagation. When $\Delta D$ = 900 nm >> 350 nm, however, the real propagation constants become almost identical for the two modes while the imaginary parts differ dramatically. Consequently, the beating period becomes overwhelmingly large and the symmetric mode decays much faster than the anti-symmetric mode. Therefore, after a certain amount of propagation distance, only the anti-symmetric mode survives. Below the symmetry breaking threshold (0< $\Delta D$ < 350 nm), power flow exists in both channels at an equal amount, regardless of the input channel. However, beyond the PT-symmetry breaking threshold, the power flows mostly through channel 2, even when the input is given only at channel 1. We should note that this does not necessarily mean that there is no power flow through channel 1. The cross-sectional power profile along the x-axis is obtained from the field profile given in Fig. 3(c).
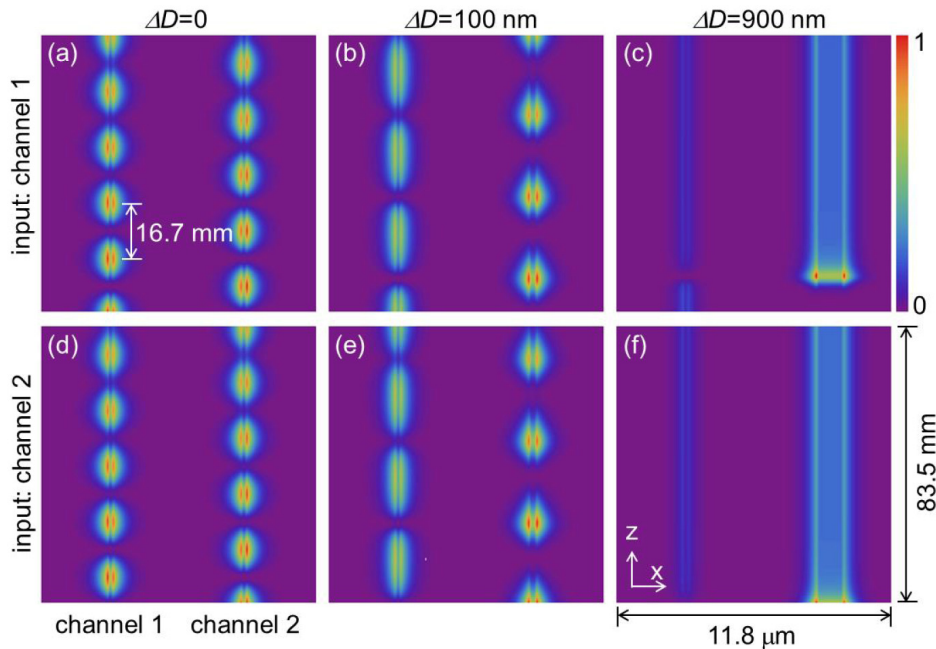


Fig. 4. State evolution during propagation along + z-direction. The three columns are for the cases where (a and d) $\Delta D$ = 0, (b and e) 100 nm, and (c and f) 900 nm. Initial state is given at channel 1 in the upper images and at channel 2 in the lower images. The power oscillation period is 16.7 mm for $\Delta D$ = 0.

Finally, we discuss the power attenuation properties of our system. Figure 5 shows the transmittance for four combinations of input-output channels as a function of $\Delta D$. Here, the channel length is fixed at 16. 7 mm which is the beating period of $\Delta D$ = 0. Around $\Delta D$ = 150 nm, there is a transmission dip (~40 dB) only for 2→2 transfer. This feature is a general aspect in passive PT-symmetric systems. The first passage length for the inter-channel power transfer varies with two major factors. They are increasing non-orthogonality between the eigen modes and change in the beat length with merging real eigen values near the exceptional point. This effect is explained in greater details by Ref [24]. We note that the transmittance of our system is quite small because both channels experience only loss and no gain. This can be alleviated by either increasing the beating period with a larger separation gap between the two channels or by reducing the loss with a wider core diameter.
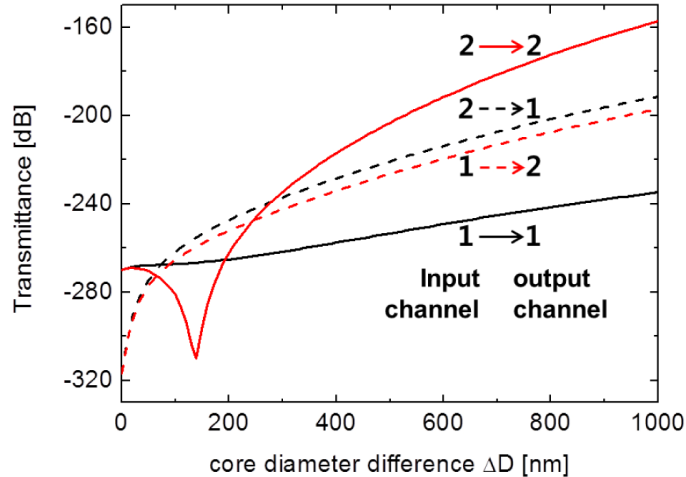
Fig. 5. Transmittance as a function of *ΔD* for four input-output channel combinations.

## 5. Conclusions and discussions

We have proposed DS-SPP coupled-waveguide structures for demonstrating spontaneous PT-symmetry breaking. We theoretically show that increasing the core thickness of either DS-SPP waveguide in the coupler causes the imaginary index of the flat-top modes to be antisymmetric while maintaining a symmetric real-index. This effect results in the robust PT phase transition by independently tuning the major symmetry-braking parameters governing the coupling processes.

One can easily tune the critical wavelength of the flat-top modes by changing the thickness of the metal slabs and/or permittivity of the dielectrics. A gain medium, as the core of the dielectric, may be introduced to realize active PT-symmetry breaking behavior, where external pumping on either of the two DS-SPP waveguides produces a spontaneous breaking in PT-symmetry once the inherent loss of the metallic channels has been compensated for. Therefore, DS-SPP waveguide couplers possessing these abilities for tuning the symmetry in the complex index represent a good method for investigating the underlying physics of PT-symmetry breaking in non-Hermitian Hamiltonian systems. In addition, the proposed DS-SPP coupled-waveguide system is favorable for adding active optical effects such as electro-optic effect and thermo-optic effect. In the proposed system, the metal films that provide the main guiding mechanism can simultaneously serve as electrodes for voltage bias and current injection. Thereby, further study with these active optical effects is of great interest for electrically controllable PT-symmetric optics.